Macromolecules
ARTICLE

Macromolecules **2010**, *43*, 8619–8627 **8619**
DOI: 10.1021/ma101625h

Effect of Substrate on the Isothermal Crystallization Kinetics of Confined Poly(ε-caprolactone) Nanolayers

Michael Ponting, Yijian Lin, Jong K. Keum, Anne Hiltner, and Eric Baer*

Department of Macromolecular Science and Engineering, Case Western Reserve University, Cleveland, Ohio 44106

Received July 19, 2010; Revised Manuscript Received September 8, 2010

ABSTRACT: Layer multiplying coextrusion was used to create films with hundreds or thousands of alternating layers of two polymers. The constituent polymers were chosen to create a temperature window in which a crystallizable polymer could melt and recrystallize within the glassy confinement of an amorphous polymer. This enabled the study of polymer crystallization behavior under nanoscale confinement. In this article, we examined the crystallization of poly(ε-caprolactone) (PCL) confined by polystyrene and poly(methyl methacrylate). We used AFM, WAXS, and SAXS to demonstrate that confined PCL nanolayers crystallized as large in-plane lamellae of high aspect ratio. This phenomenon, previously observed only for poly(ethylene oxide) (PEO), may be more general to crystalline polymers. We found that the in-plane PCL lamellae were at least as effective as PEO lamellae in reducing the oxygen permeability by more than 2 orders of magnitude. The substrates examined did not affect the crystallization habit of PCL but surprisingly had a large effect on the crystallization kinetics. The results supported the hypothesis that heterogeneous nuclei could diffuse to the interface from the confining polymer during melt processing, thereby substantially increasing the crystallization rate. In the absence of these additional nuclei, the crystallization kinetics was quantitatively described by a model that considered truncation of the growing spherulite. The retardation in crystallization rate over a very large range in layer thicknesses was described by the change in layer thickness only without any change in the linear growth rate. To our knowledge, this is the first time that the model has been quantitatively verified by experiment.

Introduction

The growing use of polymers as ultrathin films has stimulated considerable interest in understanding how reducing at least one dimension to the nanoscale impacts polymer crystallization behavior. The 1-dimensional confinement is conventionally achieved with a spin-coated thin layer on a substrate,[1] with a block copolymer that contains at least 1-crystallizable block,[2] or with a patterned substrate.[3] We recently demonstrated layer-multiplying coextrusion as a complementary method for studying polymer crystallization under long-range, almost defect-free confinement.[4,5] The advantages include the true 1-dimensional confinement, the flexibility in the choice of confined and confining polymers, and the use of conventional methods of polymer analysis to probe size-scale-dependent properties.

The coextrusion approach enabled the recent discovery that nanolayers of PEO crystallize as in-plane lamellae that resemble the PEO single crystals grown from dilute solution.[6] The high aspect ratio of the oriented lamellae imparts multiple orders of magnitude reduction in the gas permeability.[7] To date, studies that exploit layer-multiplying coextrusion to study in-plane lamellar crystals focused on poly(ethylene oxide) (PEO) exclusively. It seems likely that similar behavior occurs in other crystalline polymers. Additional examples of in-plane lamellae that impart a substantial reduction in the gas permeability are needed to establish the generality of the phenomenon and to assess the potential applications.

Even in nanolayers, it is found that crystallization of the PEO single lamellae follows the conventional habit whereby chains fold back and forth in the crystal with a common fold surface free energy and fold length.[8] Although crystallization is dramatically retarded as the layers become thinner, the Avrami equation, expressed for heterogeneously nucleated bulk crystallization, is valid for thin and ultrathin confined layers. A measured decrease in the overall crystallization rate is given a new and straightforward explanation based on area nucleation density.[8] However, the observed crystallization rate is higher than predicted by a model that considers truncation of the growing spherulites. The discrepancy increases as the layers become thinner. One hypothesis is that additional heterogeneous nuclei diffuse to the PEO layers from the confining layers during melt processing.

A candidate polymer to address these issues in confined crystallization was sought. It is reported that poly(ε-caprolactone) (PCL) blocks crystallize as in-plane lamellae when confined in a block copolymer.[9,10] Noting that the crystallinity of PCL (~40%) is substantially lower than the crystallinity of PEO (~70%), we chose PCL as a candidate for coextrusion. We probed the heterogeneously nucleated crystallization of confined PCL using two amorphous substrates: polystyrene (PS) and poly(methyl methacrylate) (PMMA). Commercial PMMA resins are reported to have very low levels of additives or stabilizers, < 50 ppm; in contrast, PS contains thermal and UV stabilizers at much higher concentrations. This enables us to test the hypothesis that diffusion of nuclei from the confining polymer causes discrepancies between experiment and model previously observed with PEO.

Materials and Methods

Materials. PCL with a reported molecular weight of 120 kg/mol[11] (Capa 6800, MFI = 7.3 g/10 min, 190 °C/2.16 kg) was

*Corresponding author. E-mail: exb6@case.edu.

Published on Web 09/28/2010

Table 1. Characteristics of PS/PCL Nanolayered Films

number of layers	PS/PCL composition (v/v)	film density (g/cm^3)	film thickness (μm)	PCL nominal layer thickness (nm)	f_{110}	film $P(O_2)$ (barrers)	$P_{PCL,eff}$ (barrers)	$X_{c,PCL}$ (wt %)	α
PS	100/0	1.045 ± 0.001	51			2.200 ± 0.200			
PCL	0/100	1.136 ± 0.001	51			0.970 ± 0.030		48	
17	50/50		250	16000	−0.03	1.397 ± 0.001	1.023	44	
17	25/75		117	11000					
17	25/75		51	4800	0.16	0.990 ± 0.020	0.837	42	
17	75/25		116	3600		1.124 ± 0.021	0.456		
17	75/25		61	1900	0.14	0.982 ± 0.029	0.369	41	
257	25/75		290	1700		0.203 ± 0.018	0.156		
257	25/75		153	900	0.26	0.155 ± 0.001	0.118	42	
257	25/75		102	600		0.101 ± 0.004	0.077		
257	50/50		102	400					
257	75/25		135	260	0.63	0.131 ± 0.001	0.034	41	
257	75/25		127	250					
1025	25/75		152	220					
257	50/50		51	200	0.67	0.059 ± 0.006	0.030	40	
257	50/50		19	75					
1025	50/50	1.086 ± 0.002	66	65	0.81	0.027 ± 0.003	0.014	42	125
257	75/25		25	50					
1025	50/50	1.085 ± 0.002	40	40	0.81	0.007 ± 0.001	0.004	42	250
1025	50/50	1.087 ± 0.001	37	35	0.77	0.005 ± 0.001	0.003	45	270

Table 2. Characteristics of PMMA/PCL Multilayered Films

number of layers	PMMA/PCL composition (v/v)	film thickness (μm)	PCL nominal layer thickness (nm)	f_{110}	film $P(O_2)$ (barrers)	$P_{PCL,eff}$ (barrers)	$X_{c,PCL}$ (wt %)
PMMA	100/0	51			0.057 ± 0.001		
PCL	0/100	51			0.970 ± 0.030		48
17	25/75	75	7000				
257	25/75	154	900	0.28	0.200 ± 0.001	1.221	43
257	25/75	127	750				
257	25/75	102	600	0.31	0.181 ± 0.001	0.659	49
257	50/50	102	400	0.29	0.085 ± 0.001	0.167	45
257	50/50	64	250		0.066 ± 0.001	0.078	
257	50/50	46	180		0.059 ± 0.005	0.061	
257	75/25	86	170	0.63	0.053 ± 0.005	0.044	
257	25/75	25	150				
257	90/10	145	110	0.53	0.055 ± 0.003	0.042	40
257	50/50	20	80		0.025 ± 0.001	0.016	
257	90/10	84	65	0.71	0.034 ± 0.005	0.007	25
257	75/25	25	50				
257	90/10	38	30	0.76	0.022 ± 0.003	0.003	26

obtained from Perstorp UK Ltd. PS (Styron 615APR, MFI = 14.0 g/10 min, 200 °C/5.0 kg, ASTM D1238) was obtained from The Dow Chemical Company. PMMA (Plexiglas VM, MFI = 14.5 g/10 min, 200 °C/5.0 kg, ASTM D1238) was obtained from Arkema Inc. The PS and PMMA were dried under vacuum at 80 °C for 12 h, and the PCL was dried under vacuum at ambient temperature for 12 h prior to viscosity measurements or film coextrusion.

To ensure polymer material rheological compatibility for coextrusion and maximize layer uniformity and overall film quality, a viscosity-match temperature for coextrusion was determined for PCL, PS, and PMMA. Polymer melt viscosity was determined as a function of temperature using a Kayeness Galaxy 1 melt flow indexer (MFI) at a low shear rate, 10 s^{-1}. This low shear rate was selected to simulate polymer flow conditions in the layer multiplying dies of the polymer melt streams during the layer multiplication process. A coextrusion temperature of 200 °C was selected for PCL and PS or PMMA based on similar measured rheological behavior at this shear rate.

Films with alternating PCL/PS or PMMA layers were fabricated using a forced assembly layer-multiplying coextrusion process.[12,13] The extruders, multiplier elements, and die temperatures were set at 200 °C to ensure matching viscosities of the two polymer melts during processing. The films were collected on a heated cast-film takeoff roll set at a temperature of 60 °C. Films with 17, 257, and 1025 alternating PCL and PS layers were coextruded (Table 1). Additional films with 17 and 257 alternating PCL and PMMA layers were coextruded (Table 2). The composition was varied by changing the relative pump rates of each polymeric material. In addition, the film thickness was varied from about 250 to 20 μm by increasing the takeoff speed. The nominal layer thickness, calculated from the number of layers, the composition ratio, and the film thickness, varied from micrometers to tens of nanometers (Tables 1 and 2). Control PCL, PS, and PMMA films were extruded through the layer multipliers under identical processing conditions as the PS/PCL and PMMA/PCL films.

Atomic Force Microscopy. The layered film structure was viewed by atomic force microscopy (AFM). The embedding process, the preparation of microtomed cross sections, and the imaging conditions were described previously.[7] Phase and height images were recorded simultaneously; however, the layered structure was best seen in phase images.

X-ray Diffraction. Small-angle X-ray scattering (SAXS) and wide-angle X-ray scattering (WAXS) patterns were obtained by aligning the incident X-ray beam parallel to the normal direction (ND), the extrusion direction (ED), or the transverse direction (TD) of the film. The experimental methods and analysis procedures were described previously.[7]

Oxygen Permeability. Oxygen flux $J(t)$ at 0% relative humidity, 1 atm pressure, and 23 ± 0.1 °C was measured using a MOCON (Minneapolis, MN) OxTran 2/20 unit. The instrument was calibrated at 23 °C with NIST-certified Mylar film of known oxygen transport characteristics. The polymer film specimens were carefully conditioned in the instrument, as described previously.[14] The permeability P was calculated from

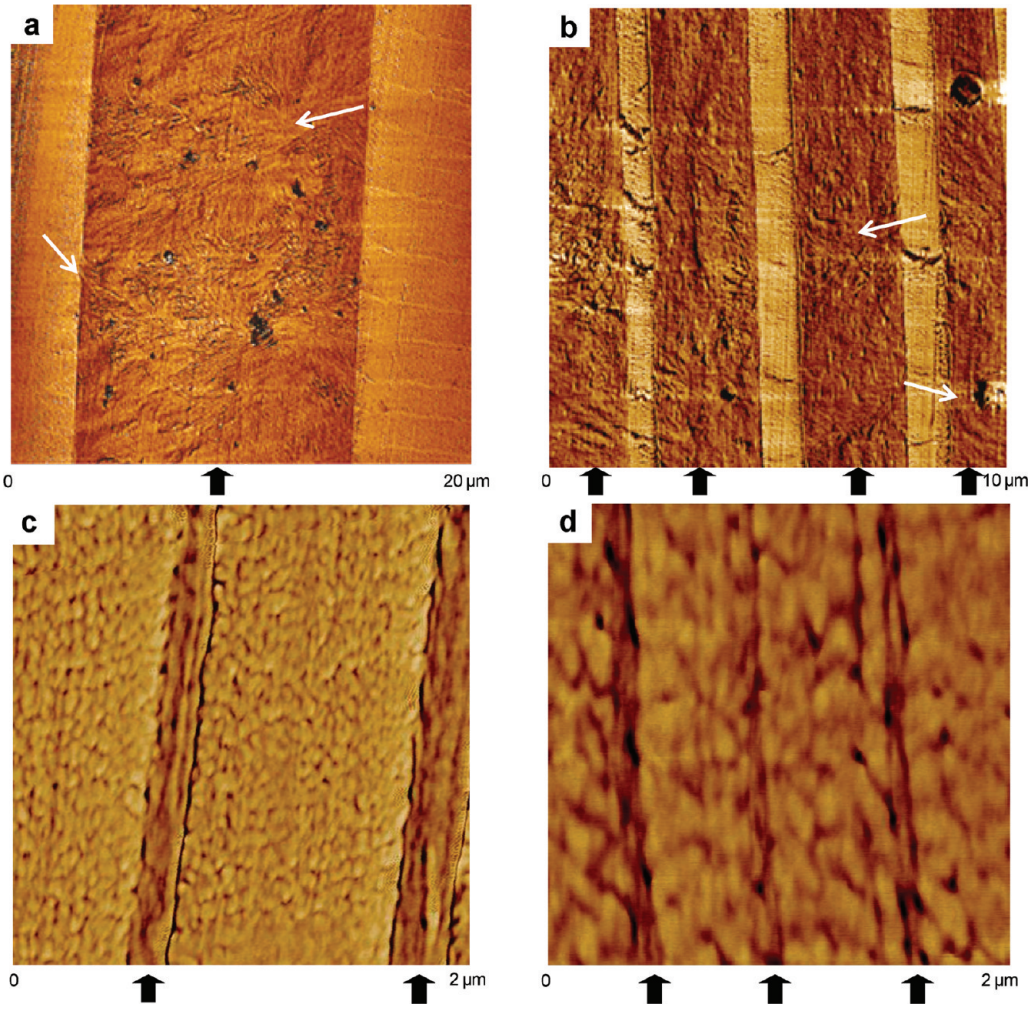

Figure 1. AFM phase images of partial cross sections of coextruded PS/PCL films with (a) 16 μm thick PCL layers, (b) 1.9 μm thick PCL layers, (c) 250 nm thick PCL layers, and (d) 50 nm thick PCL layers. Black arrows indicate the PCL layers, and white arrows indicate the center of PCL spherulites.

steady state flux J as

$$P = J\frac{l}{\Delta p} \quad (1)$$

where l is the film thickness and Δp, the difference of the oxygen partial pressure across the film, is 1 atm. For each film, the average P from a minimum of two specimens is reported (Tables 1 and 2).

Film Density. The PS/PCL film density was measured at 23 °C according to ASTM D1505-85 using an aqueous gradient density column. A water/water−calcium nitrate solution gradient column with a density range of 1.0−1.15 g/cm^3 was calibrated with known density glass floats. Small pieces of film about 2×2 mm^2 were placed in the column and allowed to equilibrate for 24 h before measurement. The average of at least three specimens is reported in Table 1.

Differential Scanning Calorimetry. The PCL crystallinity was measured on a Perkin-Elmer (Boston, MA) Series 7 differential scanning calorimeter (DSC) at a heating/cooling rate 10 °C min^{-1}. The crystallinity of the PCL control was 48 wt % calculated from the melting enthalpy using the heat of fusion of 135.5 J/g for the PCL crystal.[15] The crystallinity of the PCL layers was calculated based on the melting enthalpy of the PCL layers and the PCL weight content in the film (Tables 1 and 2).

For isothermal crystallization, the film was heated in the DSC to 85 °C to melt the PCL layers. At this temperature, the PCL layers were melted, but the PS layers remained in the rigid glassy state and maintained the layer integrity. The film was held at 85 °C for 10 min to ensure complete melting of the PCL, rapidly cooled to 40 °C, and isothermally crystallized for 2 h.

Results and Discussion

Structure of Confined PCL Layers. Cross-section AFM images of the PS/PCL films showed continuous PCL layers confined by PS layers. The measured layer thickness was close to the nominal layer thickness calculated from the composition, the number of layers, and the film thickness. As revealed by the AFM images in Figure 1, confined crystallization of PCL layers produced the same morphological features as previously reported for PEO,[7] despite the substantially lower crystallinity of PCL compared to PEO. Briefly, reducing the PCL layer thickness produced a gradual change in the crystalline morphology from isotropic 8−10 μm spherulites in thick 16 μm layers (Figure 1a), to truncated spherulites or discoids that frequently nucleated at the PS interface in 1.9 μm layers (Figure 1b), to stacks of lamellae oriented in the plane of the film in 250 nm layers (Figure 1c), to one or two very large in-plane lamellae as the 50 nm layer thickness approached the size scale of the lamellar thickness (Figure 1d). The layer thickness did not affect the lamellar thickness, which remained at 15−20 nm. Similar results were obtained for PMMA/PCL films (not shown). Thus, it appeared that crystallization of confined nanolayers as large in-plane lamellae was not unique to PEO. Very likely the phenomenon occurs in other crystalline polymers as well.

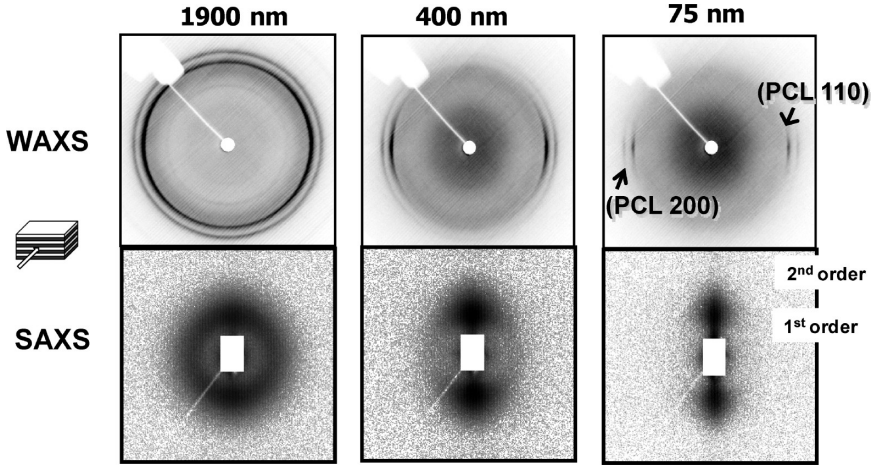

Figure 2. ED WAXS and SAXS patterns from films with 1.9 μm, 400 nm, and 75 nm thick PCL layers showing increasing in-plane PCL orientation as the layer thickness decreases from the microscale to the nanoscale.

Further studies will determine the generality of the phenomenon to crystalline polymers and will identify the characteristics that favor the in-plane crystallization habit.

The global orientation of the confined PCL layers was confirmed with WAXS and SAXS. The results were the same for PS/PCL and PMMA/PCL films, and the results for PS/PCL films are presented as representative (Figure 2). The WAXS patterns exhibited two main diffraction rings from the orthorhombic crystal structure of PCL superimposed on the broad amorphous halo of PS (2θ = 18.7°) or PMMA (2θ = 13.6°). The innermost diffraction ring (scattering angle 2θ = 21.3°) contained reflections from the PCL (110) planes, and the second ring (2θ = 23.5°) contained the PCL (200) reflections.[16] With the beam parallel to the ED, the discoidal morphology of the 1.9 μm PCL layers showed some equatorial concentration of the (110) intensity. As the constraint became more severe in 400 nm layers, the (200) and (110) diffraction intensities were concentrated in equatorial diffraction arcs. In 75 nm layers, the equatorial arcs sharpened, indicating that the chains of the in-plane lamellae were well-oriented perpendicular to the layer plane. The WAXS patterns were also obtained with the beam perpendicular to the ED and with the beam perpendicular to the film surface (ND). The TD patterns were indistinguishable from the ED patterns. The ND patterns were isotropic, suggesting that the orientation was due to confinement and was not a consequence of chain orientation during the coextrusion process.

The 2D SAXS obtained with the beam parallel to the ED showed meridional streaks; the overlapped scattering from the layer interfaces and the film surface tended to mask the scattering from the PCL lamellae. Nevertheless, the patterns revealed certain features of the lamellar orientation. The 1.9 μm layers produced a scattering ring with some concentration of intensity on the meridian. When the layer thickness decreased to 400 and 75 nm, a two-spot scattering feature emerged at the meridian. The strong meridional scattering in the ED patterns indicated that the lamellar surfaces were preferentially oriented in the plane of the layer. The appearance of spots rather than arcs in the pattern from 75 nm layers indicated a very high degree of lamellar orientation. Comparison of the meridional scattering profiles for the various layer thicknesses indicated that the first-order peak position s^* of the PCL lamellar stacks remained nearly constant. The corresponding long period $L = 1/s^*$ was 15.4 ± 0.2 nm. Here s is the scattering vector, and its amplitude is related to the scattering angle 2θ and the X-ray beam wavelength λ as $s = (\sin 2\theta)/\lambda$. Both the magnitude and the consistency of the long period agreed with the AFM results.

It is characteristic of the layered structures that the orientation function cannot be quantitatively calculated from the azimuthal intensity distribution in the ED SAXS pattern. Instead, the Hermans orientation function was obtained from the azimuthal intensity distribution of the PCL (110) reflection in the ED WAXS pattern. After the background and the amorphous contributions were subtracted, the orientation function f_{110} was calculated as[17]

$$f_{110} = \frac{3\langle \cos^2 \phi_{110} \rangle - 1}{2} \tag{2}$$

where

$$\langle \cos^2 \phi_{110} \rangle = \frac{\int_0^{\pi/2} I_{110}(\phi) \cos^2 \phi \sin \phi \, d\phi}{\int_0^{\pi/2} I_{110}(\phi) \sin \phi \, d\phi} \tag{3}$$

and $I_{110}(\phi)$ represents the corrected scattering intensity of the PCL (110) reflection at the azimuthal angle ϕ. The film plane is set as ϕ = 0°, and the normal to the film plane corresponds to ϕ = 90°; then φ_{110} is the angle between the film plane and the normal of the (110) plane. The f_{110} values from the ED WAXS patterns of PS/PCL and PMMA/PCL films are included in Tables 1 and 2, respectively. An orientation function f_{110} = 1 indicates that the normal of the (110) plane is perpendicular to the layer normal, whereas f_{110} = 0 has perfectly isotropic or random orientation. The maximum value observed was about f_{110} = 0.8. The PCL lamellae in nanolayers did not achieve as high a degree of orientation as the PEO lamellae described previously.[7] This may have been due to the higher amorphous fraction of PCL which allowed more freedom for the lamellae to tilt.

Gas Permeability of Confined PCL Layers. The oxygen permeability P of the various PS/PCL and PMMA/PCL films is tabulated in Tables 1 and 2. Comparing films with the same composition, for example 50/50 v/v, an order of magnitude decrease in P was apparent as the layer thickness decreased from micrometers to nanometers. Not only did confined PCL nanolayers crystallize as single lamellae with large aspect ratio, but this crystallization habit imparted the same dramatic reduction in oxygen permeability previously observed with confined PEO layers.

The effective permeability of the PCL layers $P_{PCL,eff}$ was calculated from the series model according to

$$P_{PCL,eff} = V_{PCL}\left(\frac{1}{P} - \frac{1 - V_{PCL}}{P_2}\right)^{-1} \quad (4)$$

where V_{PCL} is the volume fraction of PCL, P is the film permeability, and P_2 is the permeability of the confining polymer, either PS or PMMA, which is assumed to be independent of the layer thickness. An assumption of a thickness-independent amorphous layer permeability was based on keeping the amorphous PS or PMMA layers thicker or approximately equal to the PCL layer thickness by selection of unbalanced coextrusion feed ratios skewed toward more PS or PMMA, and WAXS and SAXS patterns suggesting orientation are greatly enhanced in the PCL material relative to the amorphous substrate. The PCL layer thickness was varied by changing the film thickness, the composition, and the overall number of layers in the coextruded films. Although the measured values of P scattered depending on the film composition, the results for $P_{PCL,eff}$ collapsed onto one curve for the PS/PCL films and another one for the PMMA/PCL films (Figure 3a). Only the thickest PCL layers exhibited the same permeability as the bulk, indicated by the dashed line in the plot. Deviation below the bulk value was seen with 5 μm PCL layers confined by PS and with about 1 μm PCL layers confined by PMMA. In general, obtaining the same value of $P_{PCL,eff}$ required somewhat thinner layers with PMMA constraint than with PS constraint. The maximum reduction in $P_{PCL,eff}$ was about 2.5 orders of magnitude, slightly larger than the reduction achieved with PEO nanolayers.[7]

The low permeability of the PCL nanolayers was attributed to the oriented lamellae that resulted from confined crystallization. Previously, a general correlation was established between the PEO layer permeability and the Hermans crystalline orientation function.[7] Similarly, the results for $P_{PCL,eff}$ collapsed onto a single curve when plotted as a function of f_{110} (Figure 3b).

The aspect ratio of the lamellae can be estimated using the Cussler model,[18] which considers the gas permeability of a polymer composite with a dispersion of impermeable platelets

$$P = P_M\left[1 + \frac{\alpha^2 V_p^2}{4(1 - V_p)}\cos^2\beta\right]^{-1} \quad (5)$$

where P_M is the matrix permeability, V_p is the volume fraction of impermeable platelets, α is the platelet aspect ratio, and β is the angle between the flux and the normal to the platelets, taken as 0°. The volume fraction of impermeable PCL crystals was determined from the crystallinity as

$$V_p = X_{c,PCL} W_{PCL} \frac{\rho}{\rho_{c,PCL}} \quad (6)$$

where $X_{c,PCL}$ is the crystallinity of the PCL layer measured by DSC (Table 1), W_{PCL} is the weight fraction of PCL in the layer, ρ is the measured PS/PCL film density, and $\rho_{c,PCL}$ is the PCL crystal density, 1.17 g/cm^3.[19] The aspect ratio of the in-plane lamellae was at least as large as that reported previously for PEO lamellae. Estimating the lamellar thickness to be about 6 nm from the long spacing and the crystallinity, the lateral dimension of the large lamellae was in the range 0.75−1.6 μm.

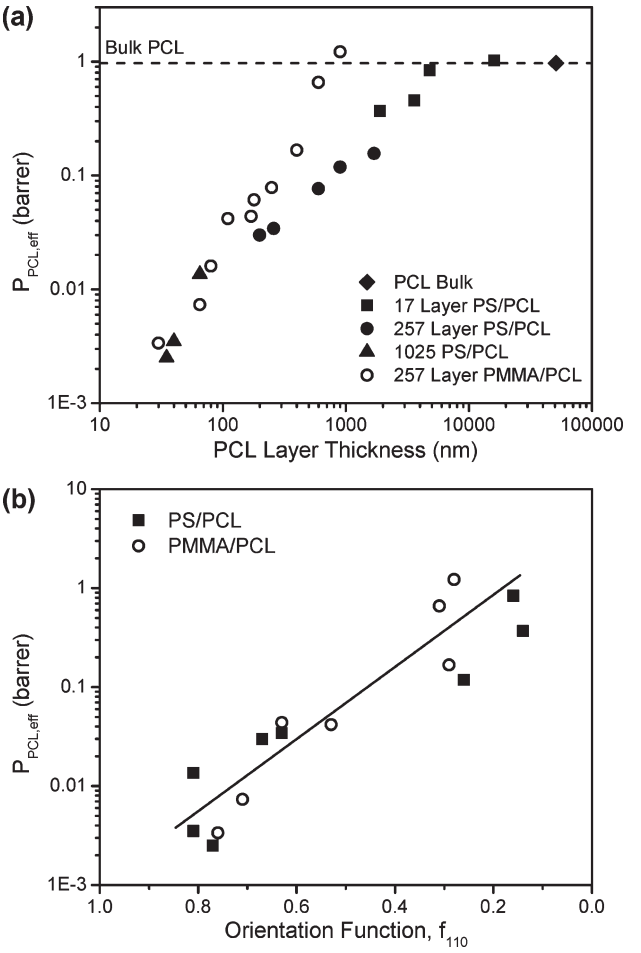

Figure 3. Effect of layer thickness on the effective permeability of the PCL layers: (a) the decrease in $P_{eff,PCL}$ as the layer thickness decreases from the microscale to the nanoscale; (b) the correlation between $P_{eff,PCL}$ and the orientation function for PS/PCL and PMMA/PCL. The solid line is drawn as a guide.

Crystallization Kinetics. A temperature window was defined in which the PCL layers could be melted within the rigid confinement of the glassy confining layers. The heating thermogram of a PS/PCL film with 50 nm PCL layers showed a melting endotherm for PCL at about 61 °C ($T_{m,PCL}$) (Figure 4). The PCL melting temperature and the PCL crystallinity of about 40% from ΔH did not vary much with the layer thickness. A baseline inflection at a higher temperature corresponded to the glass transition of PS ($T_{g,PS}$). There was a temperature window between $T_{m,PCL}$ and $T_{g,PS}$ where the PCL layers melted within the rigid confinement of the glassy PS ($T_{g,PS}$ = 101 °C). A similar window existed for the PMMA/PCL films ($T_{g,PMMA}$ = 95 °C). When the film was taken to 85 °C, within the window between $T_{m,PCL}$ and $T_{g,PS}$, and subsequently cooled at 10 °C/min, the crystallization exotherm appeared at 26 °C, only 4 °C lower than the crystallization temperature of the PCL control. A crystallization temperature close to that of the bulk and much higher than that of homogeneous nucleation, reportedly at −45 to −50 °C,[20] confirmed that crystallization of the PCL layers nucleated on heterogeneous nuclei even in very thin nanolayers.

The confined PCL layers were melted at 85 °C for 10 min and isothermally recrystallized at 40 °C. The isothermal DSC curves for all the layered films showed a single peak as is typical for isothermal polymer crystallization. The WAXD patterns confirmed that the in-plane lamellar orientation

isothermal crystallization. The relative crystallinity, X_t, was obtained for a range of PCL layer thicknesses according to

$$X_t = \frac{\Delta H_t}{\Delta H_\infty} = \frac{\int_0^t (\mathrm{d}H/\mathrm{d}t)\,\mathrm{d}t}{\int_0^\infty (\mathrm{d}H/\mathrm{d}t)\,\mathrm{d}t} \tag{7}$$

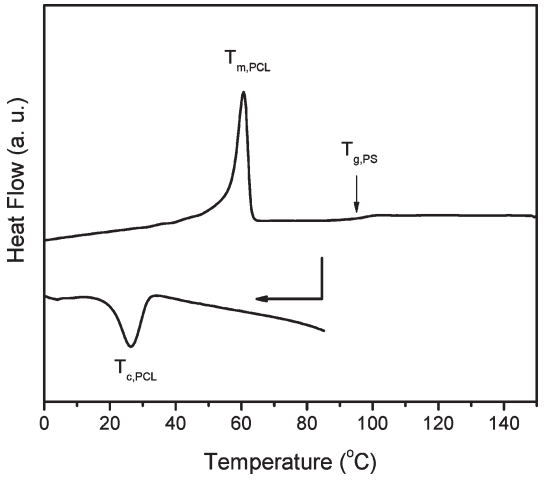

Figure 4. DSC thermogram of the PS/PCL film with 50 nm PCL layers. The heating curve was collected by heating the film to 150 °C. A second film specimen was heated to 85 °C and held for 10 min, and the subsequent cooling curve was recorded. The heating/cooling rate was 10 °C/min.

where $\mathrm{d}H/\mathrm{d}t$ is the rate of heat evolution, ΔH_t is the heat evolved at time t, and ΔH_∞ is the total heat evolved as time reaches infinity. The relative PCL crystallinity of PS/PCL and PMMA/PCL films with approximately the same layer thicknesses is plotted together with the PCL control in Figure 5. As expected, the crystallization rate decreased as the layers become thinner. Unexpectedly, the confining polymer also had a substantial effect on the crystallization rate. By plotting data for PS/PCL and PMMA/PCL on the same time scale, it is readily apparent that crystallization was much faster with PS confinement than with PMMA confinement (Figure 5a,b). The difference became increasingly noticeably as the layers became thinner. In 50 nm PCL layers the crystallization half-time more than doubled from $t_{1/2}$ = 21 min with PS confinement to $t_{1/2}$ = 50 min with PMMA confinement.

The crystallization data are plotted in Figure 5c,d according to the classic Avrami theory[21]

$$\ln[-\ln(1-X_t)] = n \ln t + \ln k \tag{8}$$

where k is the crystallization rate constant and n is the Avrami exponent describing the crystal growth geometry and nucleation mechanism. For consistency, the slope n and the intercept ln k were taken from the portion of the Avrami plot $0.05 < X_t < 0.50$. The thickness of the control film, about 50 μm, was larger than the spherulite diameter, about 14 μm, and the expected 3D spherulite growth was confirmed with an Avrami exponent of 3. Layers on the size scale of the

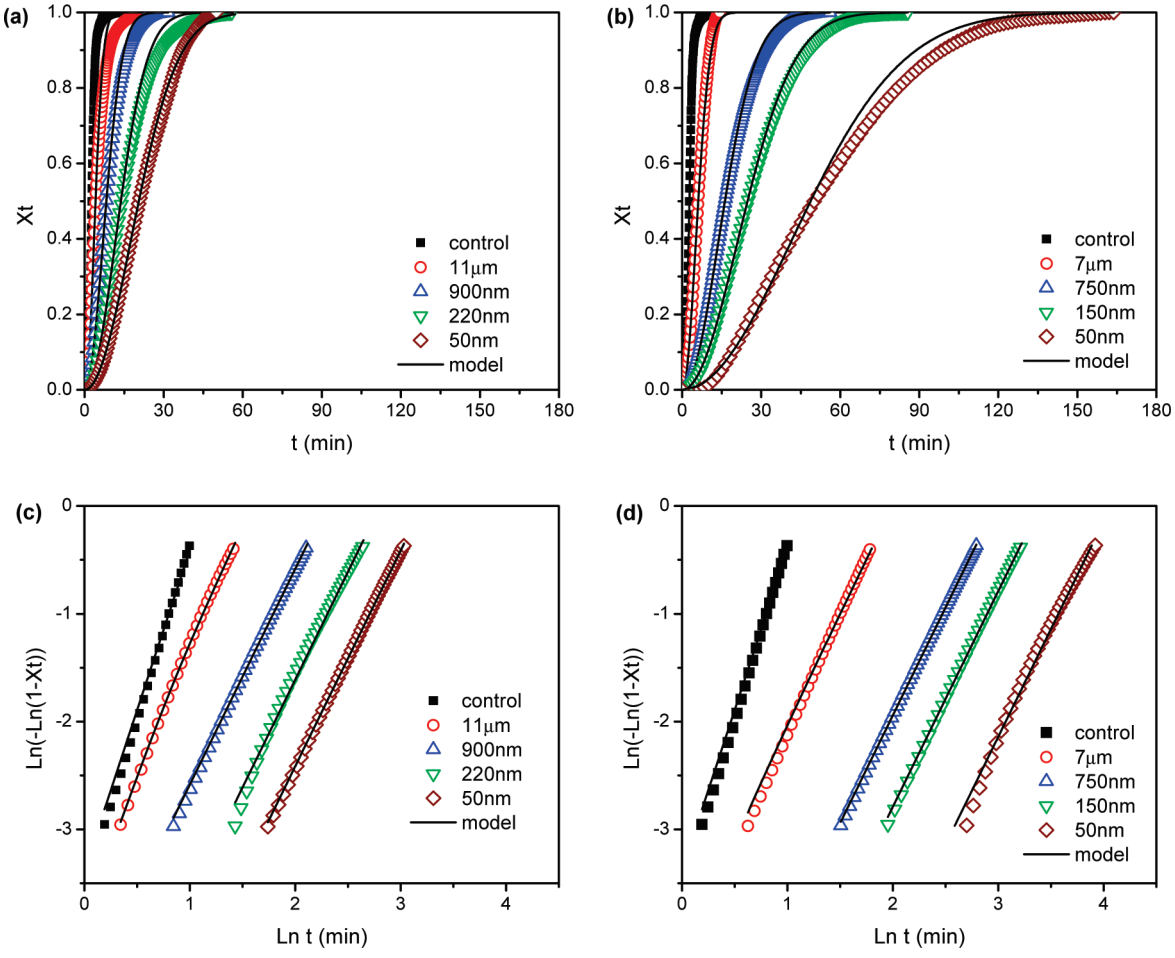

Figure 5. Relative crystallinity of PCL layers as a function of time for isothermal crystallization at 40 °C: (a) PS/PCL and (b) PMMA/PCL. Avrami plots for isothermal crystallization at 40 °C for (c) PS/PCL and (d) PMMA/PCL. The solid lines are the best fits from eqs 9 and 10.

Table 3. Kinetics Parameters for Crystallization of Confined PCL

	experimental Avrami analysis			model parameters[a]			
PCL layer thickness	n	k (min^{-1})	ΔH_∞ (J/g)	nucleation density N_v (μm^{-3}) $\times 10^5$	area nucleation density N_A (μm^{-2}) $\times 10^5$	n	k (min^{-1})
bulk PCL 51 μm	3.1	0.0271	51	7.8	862	3.0	0.034
PS/PCL films							
11 μm	2.4	0.025	49	5.6	61	2.4	0.026
900 nm	2.0	0.010	47	16.2	15	2.0	0.010
220 nm	2.0	0.003	49	23.7	5	2.0	0.004
50 nm	2.0	0.002	46	46.8	2	2.0	0.002
PMMA/PCL films							
7 μm	2.2	0.013	47	3.8	27	2.1	0.016
750 nm	2.0	0.003	47	5.0	4	2.0	0.003
150 nm	2.0	0.001	40	10.7	2	2.0	0.001
50 nm	2.0	0.0003	39	8.3	0.4	2.0	0.0003

[a] $G_0 = 4.7$ μm/min.

spherulite diameter exhibited fractional Avrami exponents, and thinner layers had Avrami coefficient of 2 for 2D growth. A decrease in the rate constant described the effect of layer thickness (Table 3). The rate constant also described the effect of the confining polymer. In the thinnest layers, crystallization against PMMA was almost an order of magnitude slower than against PS. Slower crystallization against PMMA was evident even in the thickest layers where the rate constant was about half. With the layer thickness on the micrometer scale, specific interactions with the substrate could be eliminated as the cause.

The crystallization kinetics of confined PEO layers was previously modeled by considering the effect of truncation when the growing spherulite encountered the interface.[22] The model of Haudin and co-workers predicts substantial reductions in both the crystallization rate and the Avrami exponent when the film thickness is less than the average size of the spherulite. For a thin confined layer with thickness d, the relative crystallinity X_t for instantaneous heterogeneous nucleation can be calculated from the radial growth rate of the spherulite G_0 and the initial number of potential nuclei per unit volume N_v as follows:

$$\text{for } t < d/G_0: \qquad X_t = 1 - \exp\left[-\frac{4}{3}\pi N_V {G_0}^3 t^3 \left(1 - \frac{3G_0}{8d}t\right)\right] \tag{9}$$

$$\text{for } t \geq d/G_0: \qquad X_t = 1 - \exp\left[-\pi N_v d\left({G_0}^2 t^2 - \frac{d^2}{6}\right)\right] \tag{10}$$

It should be noted that the model can give noninteger values of the Avrami exponent n. The growth rate is described with three parameters: G_0, N_v, and d. Ideally, G_0 and N_v should not depend on the layer thickness, and the retardation in crystallization rate should be described by d only. However, in the previous analysis of confined PEO crystallization, a substantial increase in N_v was required to reconcile the model with the experiments.[8] It was suggested that additional heterogeneous nuclei diffused to the PEO layers from the confining PS layers during melt processing. Concentration of nuclei would have become more important as the layers were made thinner.

Following the previous approach, the initial values of N_v and G_0 were obtained from analysis of the isothermally crystallized PCL control film. An average spherulite radius of 14.5 μm gave a nucleation density of $N_v = 7.8 \times 10^{-5}$ μm^{-3}. For $d = 51$ μm, the best fit to the kinetic data for $0.05 < X_t < 0.50$ gave $G_0 = 4.7$ μm/min at 40 °C and $n = 3$ for 3D spherulitic growth. The reported growth rate of PCL at 40 °C is 4.5−10 μm/min.[23−25]

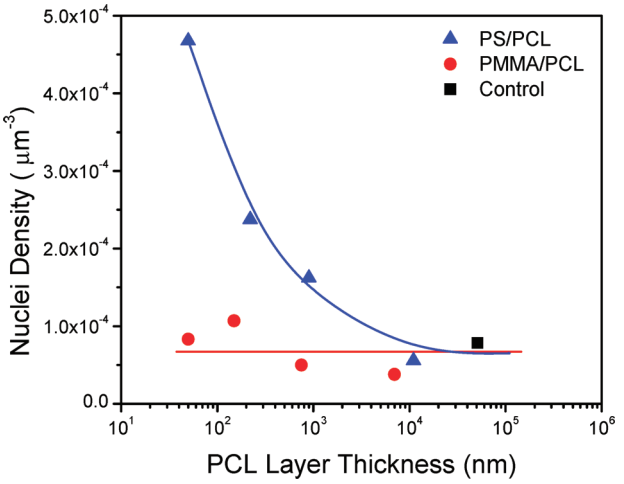

Figure 6. Values of N_v that were used in Figure 5 to obtain the best fit to eqs 9 and 10.

For the PCL layers confined by PS, the model predicted crystallization rates that were considerably slower than the observed rates if the values of G_0 and N_v obtained from the control were used and d was taken as the nominal layer thickness. Therefore, N_v was adjusted to give the best fit to the experimental data for constant $G_0 = 4.7$ μm/min (solid lines in Figure 5). Good fits for $0.05 < X_t < 0.50$ were obtained, giving a fractional Avrami exponent for the thickest layers and an Avrami exponent of 2 for thinner layers. The resulting N_v increased systematically as the layers became thinner (Figure 6). The area density of nuclei in the PCL layer defined as $N_A = N_v d$ is included with N_v in Table 3. Although N_v increased substantially as the layers became thinner, N_A decreased by an order of magnitude. Decreasing N_A facilitated formation of the large, oriented lamellae that enhanced the gas barrier of thin and ultrathin layers.

The data for PCL layers confined by PMMA were analyzed in the same way using the same values of N_v and G_0 obtained from the PCL control. In contrast to the PS/PCL films, the model described the crystallization of PCL layers confined by PMMA satisfactorily without changing N_v or G_0. When N_v was adjusted to obtain the best fit with the experiments, N_v showed no systematic changes with layer thickness, and the average value of 7.1×10^{-5} μm^{-3} for N_v was essentially the same as the control value (Figure 6).

The in-plane lamellae nucleate on heterogeneous nuclei, such as catalyst residue, high molecular weigh gel particles,

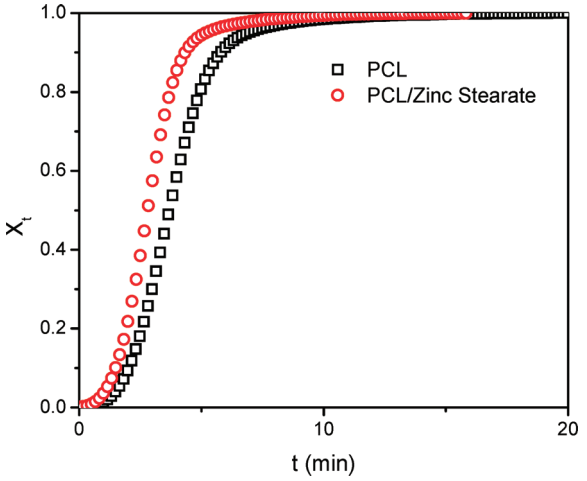

Figure 7. Effect of 0.1 wt % zinc stearate on PCL relative crystallization at 40 °C.

or dust particles. Commercial PMMA resins are reported to have very low levels of additives or stabilizers, <50 ppm; in contrast, PS contains thermal and UV stabilizers at much higher concentrations. Energetic advantages favor concentration of impurities at the layer interfaces. Indeed, it appears that except in very thick layers, crystallization tends to nucleate at the interface. Despite the substantial increase in N_v in layers confined by PS, N_A decreases with layer thickness which facilitates the formation of large in-plane lamellae.

Verification of the PS additives as heterogonous nuclei for PCL was investigated by blending PCL and a common PS processing additive, zinc stearate. Zinc stearate was blended into PCL in a twin-screw extruder at 0.1 wt % to mimic the additive levels in commercial PS resins. A blank PCL control was also processed in the twin-screw extruder to allow for comparisons of PCL samples with an identical thermal history. The blank PCL control and blend PCL with zinc stearate isothermal crystallization behavior was measured in the DSC via an identical process as previously described for the multilayered PCL/PS or PCL/PMMA films. The relative bulk PCL crystallinity versus time behavior of the PCL blank and the PCL with 0.1 wt % zinc stearate clearly displayed faster crystallization with addition of the zinc stearate additive (Figure 7). The nucleating effect of the additive reduced the crystallization half-time of the blank PCL from $t_{1/2}$ = 3.6 min to $t_{1/2}$ = 2.8 min with addition of only 0.1 wt % zinc stearate. Further analysis of the isothermal crystallization behavior of the zinc stearate nucleated PCL showed no change in the Avrami exponent, n = 3.0 for both the PCL blank and PCL with additive, indicating the nucleation effects of the additive only increased the crystallization rate without effect the crystallization mechanism or habit.

Conclusions

The ability to control the crystallization habit of polymers in confined nanolayers opens opportunities to tailor the polymer properties and to achieve property enhancements that are not possible with the bulk. For example, confined crystallization of PEO nanolayers as large in-plane lamellae dramatically increases the gas diffusion pathway, resulting in multiple orders of magnitude reduction in gas permeability compared to the bulk. Here we demonstrate that this crystallization habit is not unique to PEO. Nanolayers of PCL also crystallize as in-plane lamellae that impart a similar reduction in the gas permeability. In the thinnest nanolayers, the single lamellae may have a lateral dimension larger than 1 μm. The flexibility of the coextrusion process can be exploited further to establish the broader generality of the phenomenon and to further elucidate the factors that control the crystallization habit of candidate polymers in confinement.

We also find that the substrate can impact confined crystallization. Although our study of PCL confined by two different glassy substrates revealed only modest differences in the crystallization habit and gas permeability, surprisingly, the choice of substrate dramatically affected the crystallization kinetics. We demonstrate that our previous attempt to study the heterogeneously nucleated crystallization kinetics of confined nanolayers was flawed by diffusion of additional nuclei from the confining polymer to the interface during melt processing. By using a confining polymer with a very low level of additives and stabilizers, we showed that the crystallization kinetics was quantitatively described by an Avrami approach modified for truncated growth. The retardation in crystallization rate over a very large range in layer thicknesses, from the bulk to 50 nm, was described by the change in layer thickness only without any adjustment to the nucleation density or linear growth rate. This may be the first time that this model has been quantitatively verified by experiment.

Acknowledgment. This research was generously supported by the National Science Foundation through the Center for Layered Polymeric Systems (CLiPS) Science and Technology Center Grant DMR-0423914.

References and Notes

(1) Frank, C. W.; Rao, V.; Despotopoulou, M. M.; Pease, R. F. W.; Hinsberg, W. D.; Miller, R. D.; Rabolt, J. F. *Science* **1996**, *273*, 912.
(2) Zhu, L.; Cheng, S. Z. D.; Calhoun, B. H.; Ge, Q.; Quirk, R. P.; Thomas, E. L.; Hsiao, B. S.; Yeh, F. J.; Lotz, B. *J. Am. Chem. Soc.* **2000**, *122*, 5957.
(3) Hu, Z.; Baralia, G.; Bayot, V.; Gohy, J.-F.; Jonas, A. M. *Nano Lett.* **2005**, *5*, 1738.
(4) Jin, Y.; Roganova, M.; Hiltner, A.; Baer, E.; Nowacki., R.; Galeski, A.; Piorkowska, E. *J. Polym. Sci., Part B: Polym. Phys.* **2004**, *42*, 3380.
(5) Bernal-Lara, T. E.; Liu, R. Y. F.; Hiltner, A.; Baer, E. *Polymer* **2005**, *46*, 3043.
(6) Wang, H. P.; Keum, J. K.; Hiltner, A.; Baer, E.; Freeman, B.; Rozanski, A.; Galeski, A. *Science* **2009**, *323*, 757.
(7) Wang, H. P.; Keum, J. K.; Hiltner, A.; Baer, E. *Macromolecules* **2009**, *42*, 7055.
(8) Wang, H. P.; Keum, J. K.; Hiltner, A.; Baer, E. *Macromolecules* **2010**, *43*, 3359.
(9) Mareau, V. H.; Prud'homme, R. E. *Macromolecules* **2005**, *38*, 398.
(10) Sun, Y. S.; Chung, T. M.; Li, Y. J.; Ho, R. M.; Ko, B. T.; Jeng, U. S.; Lotz, B. *Macromolecules* **2006**, *39*, 5782.
(11) Perstrorp Inc., Biodegradable Capa Thermoplatics Datasheet, **2003**.
(12) Mueller, C. D.; Nazarenko, S.; Ebeling, T.; Schuman, T. L.; Hiltner, A.; Baer, E. *Polym. Eng. Sci.* **1997**, *37*, 355.
(13) Ponting, M.; Hiltner, A.; Baer, E. *Macromolecular Symposia* **2010**, *294*, 19.
(14) Sekelik, D. J.; Stepanov, E. V.; Nazarenko, S.; Schiraldi, D.; Hiltner, A.; Baer, E. *J. Polym. Sci., Part B: Polym. Phys.* **1999**, *37*, 847.
(15) Crescenze, V.; Manzini, G.; Calzolari, G.; Borri, C. *Eur. Polym. J.* **1972**, *8*, 449.
(16) Bittiger, H.; Marchessault, R. H.; Niegisch, W. D. *Acta Crystallogr.* **1970**, *B26*, 1923.
(17) Hermans, P. H. *Contribution to the Physics of Cellulose Fibres*; Elsevier: Amsterdam, 1946; p 195.

(18) Cussler, E. L.; Hughes, S. E.; Ward, W. J., III; Aris, R. *J. Membr. Sci.* **1998**, *38*, 161.
(19) Lefevre, C.; Villers, D.; Koch, M. H. J.; David, C. *Polymer* **2001**, *42*, 8769.
(20) Müller, A. J.; Balsamo, V.; Arnal, M. L.; Jakob, T.; Schmalz, H.; Abetz, V. *Macromolecules* **2002**, *35*, 3048.
(21) Avrami, M. *J. Chem. Phys.* **1939**, *7*, 1103.
(22) Escleine, J. M.; Monasse, B.; Wey, E.; Haudin, J. M. *Colloid Polym. Sci.* **1984**, *262*, 366.
(23) Chen, Y. F.; Woo, E. M. *Colloid Polym. Sci.* **2008**, *286*, 917.
(24) Du, Z. X.; Yang, Y.; Xu, J. T.; Fan, Z. Q. *J. Appl. Polym. Sci.* **2007**, *104*, 2986.
(25) Chen, H. L.; Li, L. J.; Yang, W. C. O.; Hwang, J. C.; Wong, W. Y. *Macromolecules* **1997**, *30*, 1718.